A ROBUST DIGITAL AUTOPILOT FOR SPACECRAFT EQUIPPED WITH PULSE-OPERATED THRUSTERS

Sam W. Thurman"
Jet Propulsion Laboratory, Pasadena, California
and
Henryk Flashner**
University of Southern California, Los Angeles, California

The analysis and design of attitude control systems for spacecraft employing pulse-operated (on-off) thrusters is usually accomplished through a combination of modeling approximations and empirical techniques. in this paper a new thruster pulse-modulation scheme for pointing and tracking applications is developed from nonlinear control theory. This scheme forms the basis of an autopilot suitable for usc in digital computers whose performance and robustness properties arc characterized analytically, in the design process. Given bounds on the anticipated dynamical modeling errors and sensor errors, it is shown that design specifications can bc established and acceptable performance ensured in the presence of these error sources. The autopilot can accommodate spacecraft with time-varying inertia properties, and is equally applicable to thruster configurations in which engines arc clustered together to provide multiple discrete torque levels about onc or more spacecraft axes. A realistic application of the theory is illustrated via detailed computer simulation of a digital autopilot designed for midcourse guidance of a hypothetical interplanetary spacecraft

---

" Graduate Student, Department of Aerospace Engineering, University of Southern California, University Park, Los Angeles, California 90089, and Member Technical Staff, Mars Pathfinder Project, Jet Propulsion 1 aboratory, 4800 Oak Orove Dr., Pasadena, California 91109. Senior Member AIAA

** Associate Professor, Departments of Mechanical and Aerospace Engineering, University of Southern California, University Park, Los Angeles, California 90089. Member AIAA

INTROD1JC"I'1ON

The analysis and design of three-axis attitude control systems for spacecraft presents a challenging problem due to the nonlinear nature of their dynamics, Even in circumstances where linear approximations are valid, the use of pulse-operated (on-off) thrusters for actuation results in control systems that arc inherently nonlinear. Onc of the earliest and most widely used design approaches in this case is to assume that the equations of motion arc uncoupled, a reasonable approximation for small rotation rates, and employ phase-plane analysis techniques to establish empirical switching curves' or to develop control laws that modulate thruster pulse width or frequency to obtain a quasi-proportional response.[2] Phase-plane techniques also permit an approximate assessment of limit cycle behavior and the effects of disturbance torques and sensor noise.[1-4] This approach has been used to develop the attitude control systems of space vehicles as diverse as the *Apollo* spacecraft,[5, 6] the *Viking* Mars lander,[7] and the Space Shuttle.[8] Sophisticated computer simulations were developed and used extensively in the design of these vehicles, to validate the approximations employed

in missions requiring slewing over large angles, Euler's rotation theorem, which specifics that any altitude change of a rigid body can bc accomplished by a rotation about an axis fixed with respect to both the vehicle and inertial space, provides a useful and efficient basis for performing these maneuvers, The dynamical coupling inherent in this approach has previously been dealt with in several different ways, such as slewing at small rotation rates to minimize coupling effects,[8] open-loop implementation of a precomputed angular acceleration profile,[9] and the usc of feedback linearization to transform the original nonlinear system into an equivalent linear systcm, to which linear control theory can bc applicd,[10]14 in the feedback linearization schemes discussed in the literature, the control law obtained is a continuously time-vatying function. To mechanize this type of control law using pulse-operated thrusters, a second design problem must bc solved, that of developing a firing logic which implements the desired torque commands with acceptable accuracy.

in this paper a new pulse-~vidth pulse-frequency modulation scheme is developed for pointing and tracking applications, using a modified Euler rotation technique to align the spacecraft with a commanded attitude or attitude profile. This scheme is designed to cause the complete closed-loop system, not just the torque profile produced by the thrusters, to approximate a specified linear system. The important question of robustness is addressed directly: given upper bounds on the sources of modeling error (thrust level variations, center of mass and moment of inertia calibration errors, attitude sensing errors, etc.), design specifications can be established such that the desired performance is ensured in the presence of these error sources, This approach is derived from a robust control technique based on Lyapunov stability theory originated by Corless and Leihnann,[15]16 which was also used in previous work by the authors addressing guidance applications.[17] Similar techniques, such as sliding mode control, arc described by Utkin[18] and Slotine and Li.[19] Unlike previous approaches based on Lyapunov theory,'1-'4 this new approach provides a comprehensive evaluation of robustness properties, and allows for analytical characterization of transient error dynamics, limit cycle dcadband, and the effects of attitude and rate estimation errors,

Some spacecraft are equipped with multiple thrusters configured such that two or even three discrete torque levels can be applied to one or more body axes (the Space Shuttle is one example), In addition, the attitude control function on most modern spat.ccrafl is performed by an autopilot implemented as a sampled data system, Using the pulse-modulation scheme outlined above, an autopilot suitable for usc in digital computers is developed which is equally applicable to thruster configurations providing single or multiple torque levels. Inputs to the autopilot can take the form of a commanded attitude or a commanded attitude and rate profile. The proposed autopilot can also accommodate spacecraft with time-varying inertia properties, It is shown that the effect of sampling rate on performance can be assessed within the same analytical framework used to evaluate robustness and performance properties.

PROBLEM DEFINITION

The equations describing the rotational motion of a rigid body are well documented in texts such as those by Hughes[20] and Wertz.[21] These equations can be subdivided into two sets, the dynamical equations relating the rate of change of angular momentum to the applied torque, and a set of kinematic equations that relate some parameterization of the attitude to the angular velocity of the body. For spacecraft equipped with mass expulsion devices such as thrusters, the moments of inertia of the vehicle will be time-varying in addition to the angular momentum vector.

Designating the inertia tensor as J, the angular velocity vector as ω, and the applied torque vector as m, the dynamical equations of a rigid spacecraft expressed in a body-fixed frame are as follows:

$$\mathbf{J}\dot{\boldsymbol{\omega}} = \mathbf{m} - \dot{\mathbf{J}}\boldsymbol{\omega} - \boldsymbol{\omega} \times \mathbf{J}\boldsymbol{\omega} - \sum_{i=1}^{N} \dot{m}_i \sum_{j=1}^{3} l_{ij}^2 \omega_j \tag{1}$$

in Eq. (1), $\dot{m}_i$ is the propellant mass flow rate of the i 'i' thruster ($\dot{m}_i > 0$ by convention), l_{ij} is the perpendicular distance between the thruster and the j^{th} body reference axis, and ω_j is the component of the vector ω along the j^{th} body reference axis. The terms in this equation due to the rate of change of inertia and propellant expulsion are usually small compared with the other terms, but can be significant during large propulsive maneuvers, The applied torque vector, m, is

$$\mathbf{m} = \sum_{1=1}^{N} \mathbf{l}_i \times \mathbf{f}_i \tag{2}$$

In Eq. (2), the vector $\mathbf{l}_i$ represents the position of the i^{th} thruster relative to the center of mass of the spacecraft, and f_i is the thrust vector of the i^{th} thruster.

The thrust profile of a representative thruster firing is shown in Fig. 1. As suggested by this illustration, some thrusters can exhibit a noticeable departure from an ideal square wave profile. The ignition and termination commands are each followed by a delay due to the electrical and mechanical

operation of the propellant valves, and a thrust buildup or decay period, respectively. Typical values for these delay times and buildup and decay periods range from just a few milliseconds to several hundred milliseconds, depending upon the size and type of thruster. The steady-state thrust level also varies roughly 1 to 10 percent between successive firings, depending upon the firing period and type of thruster, with the greatest variation occurring when using very short or very long pulses,

Several different parameterizations of the spacecraft attitude can be used An Euler symmetric parameter, or quaternion, representation is one of the most useful for attitude control systems that must operate over a wide angular range,"[4] and will be employed herein. Other representations are described in available texts."[1] The four-parameter attitude quaternion, which consists of a three-element vector part and a scalar part, is specified as follows:

$$q = \left(\sin\frac{\varphi}{2}\lambda, \cos\frac{\varphi}{2}\right) \tag{3}$$

in Eq. (3), λ is a unit vector about which a rotation through the angle φ will move the designated spacecraft body-fixed coordinate frame from a nonrotating reference frame into its current orientation. The evolution of the quaternion is governed by the following differential equation:

$$\dot{q} = \tfrac{1}{2}\Omega q \tag{4}$$

where

$$\Omega = \begin{bmatrix} 0 & \omega_3 & -\omega_2 & \omega_1 \\ -\omega_3 & 0 & \omega_1 & \omega_2 \\ \omega_2 & -\omega_1 & 0 & \omega_3 \\ -\omega_1 & -\omega_2 & -\omega_3 & 0 \end{bmatrix} \tag{5}$$

in Eq. (5), the quantities ω_1, ω_2, and ω_3 are the components of the spacecraft angular velocity vector expressed in the designated body-fixed frame, i.e., $\omega = [\omega_1 \omega_2 \omega_3]^T$. Equation (4) makes use of a column

vector representation of the quaternion, q, such that $q = [q_1, q_2, q_3, q_4]^T$, where the first three elements (q_1, q_2, q_3) constitute the vector part of the quaternion, and the fourth element (q_4) is the scalar part.

A quaternion is a convenient representation for three-axis reorientation maneuvers, in which the commanded attitude is specified as a quatcmion, designated q_c, and for tracking applications, in which the commanded attitude profile is expressed as a time history, $q_c(t)$ and an associated rate profile, $\omega_c(t)$. The error quaternion, designated Aq, representing a unique rotation axis and angle needed to rotate the spacecraft from its current attitude, specified by q, into alignment with the commanded attitude q_c, can be computed using quaternion multiplication:

$$Aq = q^{-1} q_c \tag{6}$$

The inverse quaternion, q^{-1}, represents a rotation opposite that associated with the quatcmion q, and is defined as follows:

$$q^{-1} = (-\sin\frac{\varphi}{2}\lambda, \cos\frac{\varphi}{2}) \tag{7}$$

The resulting error quaternion can be written as

$$Aq = (\sin\frac{\Delta\varphi}{2}\mathbf{e}, \cos\frac{\Delta\varphi}{2}) \tag{8}$$

The unit vector c in Eq. (8) represents the axis about which a rotation of angle $\Delta\varphi$ will bring the vehicle into alignment with the commanded attitude or point along an attitude profile. For attitude control and stabilization, a feedback logic specifying the commanded torque, designated $\mathbf{m}_c$, in the form $\mathbf{m}_c = m(Aq, Ace)$, where $\Delta\omega = \omega - UC$, is sought that is compatible with the restrictions imposed by using pulse-operated thrusters, yet still achieves acceptable performance.

PULSE-MODULATION CONTROL THEORY

The proposed pulse-modulation technique consists of equations defining the commanded torque and the thruster firing logic. It is intended for spacecraft with thruster configurations that can apply torque about each axis of a designated body-fixed frame; the torques produced by the thrusters are not required to be mutually orthogonal, although this is often the case in practice. A general form for two different types of pulse-mode controllers is presented, one that contains no model parameters and the other containing feedback linearization and feedforward terms, analogous to the continuous-time control laws presented by Wen and Kreutz-Delgado[13] and Weiss[14] In the development given below, all of the quantities discussed can be time-varying unless specific restrictions are stated to the contrary.

Commanded Torque Formulation

A general form for the commanded torque vector, $\mathbf{m}_c$, that encompasses both the mode]-indcpcndcnt and model-dcpcndcnt cases is as follows:

$$\mathbf{m}_c = \hat{\mathbf{u}}(\Delta\hat{\Phi}, \Delta\hat{\omega}) + \mathbf{K}_c(\bar{\mathbf{J}}, \bar{m}_i, \bar{\mathbf{I}}_i, \hat{\omega}, \omega_c)\,\mathbf{n}[(1/\epsilon)\hat{\mathbf{v}}(\Delta\hat{\Phi}, \Delta\hat{\omega})] + \mathbf{c}(\bar{\mathbf{J}}, \bar{m}_i, \bar{\mathbf{I}}_i, \hat{\omega}, \omega_c) \qquad (9)$$

wher c

$$\Delta\hat{\Phi} = \Delta\hat{\varphi}\hat{\mathbf{e}} \qquad (10)$$

The first two terms of Eq. (9) arc intended to null attitude and rate tracking errors, while the third term represents any desired model compensation terms, designed to cancel nonlinear elements of the dynamical equations, and feedforward terms to aid in following a commanded attitude and rate profile. The vectors $\Delta\Phi, \Delta\omega$, and ω are denoted with "hat" symbols to indicate that in actual applications only estimates of these parameters, derived from sensor data onboard the spacecraft, arc used in the computations, in a similar vein, the quantities J, $\dot{m}_i$, and Ii arc denoted with overbar symbols to show that inexact estimates of these parameters arc also used, the difference being that in actual practice these

quantities arc often not estimated from sensor data (notable exceptions exist, such as adaptive controllers which attempt to estimate **J** during their operation[13]); *a priori* estimates or values computed from some nominal model arc used instead. The estimated attitude error angle and rotation axis appearing in Eq. (10) arc obtained from an estimate of the quaternion Aq defined in Eq. (8):

$$\Delta\hat{\varphi} = 2\cos^{-1}\Delta\hat{q}_4 \tag{11}$$

$$\hat{\mathbf{e}} = (1 - \Delta\hat{q}_4^2)^{-1/2}[\Delta\hat{q}_1\ \Delta\hat{q}_2\ \Delta\hat{q}_3]^T \tag{12}$$

In Eq. (12), the vector c is defined such that the rotation about this axis required to bring the spacecraft into alignment with the commanded attitude is always positive in a right-handed sense, thus the rotation angle $\Delta\varphi$ is > 0.

The vector functions $\hat{\mathbf{u}}$ and $\hat{\mathbf{v}}$ appearing in Eq. (9) consist of proportional and derivative feedback terms with the following form:

$$\hat{\mathbf{u}} = \mathbf{K}_P\Delta\hat{\boldsymbol{\Phi}} - \mathbf{K}_D\Delta\hat{\boldsymbol{\omega}} \tag{13}$$

$$\hat{\mathbf{v}} = k_P\Delta\hat{\boldsymbol{\Phi}} - k_D\Delta\hat{\boldsymbol{\omega}} \tag{14}$$

As in Eq. (9), u and v arc denoted with hat symbols in Eqs. (13) and (14), signifying that these quantities are determined from estimates of $\Delta\boldsymbol{\Phi}$ and $\Delta\boldsymbol{\omega}$, rather than their true values, when computing the commanded torque. In Eq. (13), $\mathbf{K}_P$ rind $\mathbf{K}_D$ arc constant 3 x 3 gain matrices, whereas k_P and k_D in Eq (14) arc positive, constant scalars, The matrices $\mathbf{K}_P$ and $\mathbf{K}_D$ are symmetric and positive definite, and must satisfy the following relationships with k_P and k_D:

$$\| \mathbf{K}_P \Delta\Phi \| / \bar{\sigma}(\mathbf{J}) > k_P \| \Delta\Phi \| \tag{15}$$

$$\| \mathbf{K}_D \Delta\omega \| / \bar{\sigma}(\mathbf{J}) > k_D \| \Delta\omega \| \tag{16}$$

The double linesinEqs,(15)and(16) signify the Euclidean norm of the bracketed vector, while $\bar{\sigma}(\mathbf{J})$ represents an upper bound on the largest eigenvalue of the inertia tensor, **J**. These equations require the induced norm of the matrices $\mathbf{K}_P$ and $\mathbf{K}_D$ to be large enough such that the commanded *torque* specified by the vector u will deliver, at a minimum, the angular *acceleration* specified by the vector **v**.

The 3×3 matrix $\mathbf{K}_\epsilon$ and the vector function **n** appearing in Eq. (9) arc designed to simultaneously compensate for known torque implementat ion errors duc to the usc of discrete thruster firings, and unknown or uncompensated dynamical effects; the requirements they must satisfy arc described in further detail below. The scalar parameter ϵ ultimately determines the control accuracy that can be achieved, and will also be discussed subsequently.

The third and final term appearing in Eq. (9) is the vector function c, containing model compensation and feedforward terms that may be used to improve performance and efficiency in some scenarios. The most comprehensive expression that can be employed here is as follows:

$$\mathbf{c} = \hat{\omega} \times \bar{\mathbf{J}}\hat{\omega} + \dot{\bar{\mathbf{J}}}\hat{\omega} + \sum_{i=1}^{N} \bar{m}_i \sum_{j=1}^{3} \bar{l}_{ij}^2 \hat{\omega}_j + \bar{\mathbf{J}}\dot{\omega}_c \tag{17}$$

The first three terms of Eq. (17) arc designed to cancel the gyroscopic and mass expulsion terms in the spacecraft dynamics that appear in Eq. (1). The fourth and final term represents an input torque profile to aid in tracking a commanded rate profile, if onc is desired, and its associated attitude profile. For precision tracking applications, employing all of the terms shown in Eq. (17) is not always necessary; usually only the gyroscopic term and the input torque profile arc needed.

Pulsr-Mode Controller Dynamics

Most spacecraft equipped with propulsive attitude control systems can apply a small number (perhaps one to three) of discrete torque levels to designated body axes through different combinations of thruster firings. The thruster firing logic employed herein is to select a thruster combination at each command interval that delivers the torque vector most closely matching the commanded torque, $\mathbf{m}_c$, given by Eq. (9). Equation (9) is structured such that straightforward application of this firing logic yields satisfactory performance. The actual torque applied to the vehicle at any instant therefore differs from the commanded value. The applied torque vector, m, is written as

$$\mathbf{m} = \mathbf{m}_c + \Delta\mathbf{m} + \delta\mathbf{m} \tag{18}$$

In Eq. (18), the vector Arn is equal to the difference between the command torque, $\mathbf{m}_c$, and the nearest torque value that can nominally be obtained, while the vector $\delta\mathbf{m}$ represents torque implementation errors duc to thrust level variations, thruster misalignment, calibration errors, etc. Further characterization of&n requires specific knowledge of thruster specifications and their configuration,

Substituting Eq. (18) into Eq. (1) and making usc of Eqs. (9), (13), (14), and (17) yields the following equation of motion for the closed-loop system:

$$\Delta\dot{\boldsymbol{\omega}} = \mathbf{J}^{-1}\{\mathbf{K}_P\Delta\boldsymbol{\Phi} - \mathbf{K}_D\Delta\boldsymbol{\omega} + \mathbf{K}_\epsilon\mathbf{n}[(1/c)(k_P\Delta\boldsymbol{\Phi} - k_D\Delta\boldsymbol{\omega} + \delta\mathbf{v})] + \mathbf{h}\} \tag{19}$$

where

$$\mathbf{h} = \mathbf{c} - \boldsymbol{\omega}\times\mathbf{J}\boldsymbol{\omega} - \dot{\mathbf{J}}\boldsymbol{\omega} - \sum_{i=1}^{N}\dot{m}_i\sum_{j=1}^{3}l_{ij}^2\omega_j - \mathbf{J}\dot{\boldsymbol{\omega}}_c + \Delta\mathbf{m} + \delta\mathbf{m} + \delta\mathbf{u} \tag{20}$$

In Eq. (19), the arguments of $\mathbf{K}_\epsilon$ are no longer shown for simplicity. The vectors $\delta\mathbf{u}$ and $\delta\mathbf{v}$ in Eqs. (19) and (20) represent erroneous commands induced by attitude and rate sensing errors, and arc given by

$$\delta \mathbf{u} = \mathbf{K}_P \delta\Phi + \mathbf{K}_D \delta\omega \tag{21}$$

$$\delta \mathbf{v} = k_P \delta\Phi + k_D \delta\omega \tag{22}$$

in Eqs. (21) and (22), $\delta\Phi$ and $\delta\omega$ represent attitude and rate estimation errors, respectively.

The properties required of the matrix $\mathbf{K}_\epsilon$ and the vector function $\mathbf{n}$ of Eq. (9) will now be addressed The matrix $\mathbf{K}_\epsilon$ is symmetric and positive definite; it must also satisfy the following constraint:

$$\| \mathbf{K}_\epsilon \mathbf{n} \| / \bar{\sigma}(\mathbf{J}) \geq k_\epsilon \| \mathbf{n} \| \tag{23}$$

Where

$$k_\epsilon > \| \mathbf{h} \| / \underline{\sigma}(\mathbf{J}) \tag{24}$$

The function k_ϵ appearing in Eqs. (23) and (24) is designed to ensure that the commanded angular acceleration due to the term $\mathbf{J}^{-1}\mathbf{K}_\epsilon \mathbf{n}$ in Eq. (19) will be larger than any unmodeled disturbances and uncompensated angular accelerations represented by $\mathbf{J}^{-1}\mathbf{h}$, In Eqs. (23) and (24), $\bar{\sigma}(\mathbf{J})$ and $\underline{\sigma}(\mathbf{J})$ represent upper and lower bounds on the eigenvalues of the inertia tensor, J, respectively. If needed, k_ϵ can be specified in terms of model parameters such as $\bar{\mathbf{J}}, \hat{\omega}, \dot{\omega}_c$, etc., to track dynamical variations in $\mathbf{J}^{-1}\mathbf{h}$ with the physical counterparts of these parameters, or k_ϵ can be a constant representing a global bound. Note that for a model-independent controller, in which the function c from Eq. (17) is set to zero, the vector h of Eq. (20) will be larger than it would if model compensation was employed, imposing a greater requirement on k_ϵ. The function n can be any function with the following properties:

$$\begin{aligned} &(i) \quad \| \mathbf{v} \| \mathbf{n}(\epsilon, \mathbf{v}) = \| \mathbf{n}(\epsilon, \mathbf{v}) \| \mathbf{v} \\ &(ii) \quad \| \mathbf{n}(\epsilon, \mathbf{v}) \| \geq 1 - \epsilon / \| \mathbf{v} \|; \qquad \| \mathbf{v} \| > \epsilon \end{aligned} \tag{25}$$

Stability Analysis

The stability of the system defined by Eqs. (19) through (22) will be evaluated using Lyapunov theory.[15-20] A *Lyapunov function candidate* is sought which shows that within the domain of $\Delta\Phi$ and $\Delta\omega$ all possible trajectories are *globally, uniformly, exponentially convergent* to within a small region of radius *b* around the origin ($\Delta\Phi = 0, \Delta\omega = 0$). Designating the vector $x = [\Delta\Phi\ \Delta\omega]^T$, the system is said to be exponentially convergent with rate *a* to the desired vicinity around the origin if, for some positive constant β, the following inequality is satisfied:

$$\|\mathbf{x}(t)\| \le b + \beta\|\mathbf{x}(t_o)\|\exp[-\alpha(t - t_o)]; \quad t \ge t_o \tag{26}$$

The proposed Lyapunov function candidate, designated V(x), is

$$V(\mathbf{x}) = \tfrac{1}{2}\mathbf{x}^T\mathbf{P}\mathbf{x} = \tfrac{1}{2}[\Delta\Phi^T\ \Delta\omega^T]\begin{bmatrix} k_I\mathbf{I} & -k_P\mathbf{I} \\ -k_P\mathbf{I} & k_D\mathbf{I} \end{bmatrix}\begin{bmatrix} \Delta\Phi \\ \Delta\omega \end{bmatrix} \tag{27}$$

As shown in Eq. *(27), the* matrix P is composed of four 3×3 submatrices (1 is the identity matrix). The parameters k_P and k_D *are* defined in Eqs. (15) and (1 6), respectively; k_I will subsequently be determined such that the required stability criteria are satisfied. For the system to behave according to Eq. (26), V(x) must satisfy the following conditions, as shown by Corless:[15]

$$\begin{aligned} &(\mathrm{i})\ \ c_1\|\mathbf{x}\|^2 \le \mathbf{v}(\mathbf{x}) \le c_2\|\mathbf{x}\|^2;\ c_1, c_2 > 0 \\ &(ii)\ \dot{V}(\mathbf{x}) \le -2\alpha[V(\mathbf{x}) - V^*];\ V(\mathbf{x}) > V^* \end{aligned} \tag{28}$$

Equation (28) represents a set of sufficient, not necessary, conditions. If a Lyapunov function satisfying these conditions is not found, or if for some V(x) Eq. (2.8) is violated for a specific value of x, this dots not necessarily imply that the origin of the system is *unstable*.

To satisfy condition (r') of Eq. (28), the matrix 1' of Eq. *(27)* must be positive definite, This requires that k_L and k_D arc> O, and that $k_L k_D - k_P^2 > O$. To check condition *(ii)* of Eq. (28), the derivative of V(x) is needed; this is obtained using Eqs. (27) and (19):

$$v = k_L \Delta\varphi \Delta\dot{\varphi} + k_P \Delta\dot{\varphi}^2 + (k_D \Delta\omega^T - k_P \Delta\Phi^T)\mathbf{J}^{-1}\{\mathbf{K}_P \Delta\Phi - \mathbf{K}_D \Delta\omega + \mathbf{K}_c\, n[(1/\epsilon)\hat{\mathbf{v}}] + \mathbf{h}\} \quad (29)$$

Using Eqs. (15),(16), and (23), and noting that $\Delta\Phi^T\Delta\omega = \Delta\omega^T\Delta\Phi = -\Delta\varphi\Delta\dot{\varphi}$, Eq. (29) can be shown to satisfy the following inequality:

$$\dot{V} \le -k_P^2 \Delta\varphi^2 + (k_P - k_D^2)\|\Delta\omega\|^2 + (k_L - 2k_P k_D)\Delta\varphi\Delta\dot{\varphi} - \mathbf{v}^T\{k_c\, n[(1/\epsilon)\hat{\mathbf{v}}] + \mathbf{J}^{-1}\mathbf{h}\} \quad (30)$$

in Eq. (30), $V^T = [k_P \Delta\Phi^T + k_D \Delta\omega^T]$. By comparing terms in Eqs. (27) and (30), the following formulas for k_P, k_D, and k_L arc obtained that can fulfill both conditions of Eq. (28):

$$\begin{bmatrix} k_L & -k_P \\ -k_P & k_D \end{bmatrix} = 2\alpha \begin{bmatrix} 2\alpha^2 & -\alpha \\ -\alpha & 1 \end{bmatrix} \quad (31)$$

Substitution of Eq. (31) into Eq. (30) and noting that $v = \hat{\mathbf{v}} - \delta\mathbf{v}$ leads to the following relationship between V and $\dot{V}$:

$$\dot{V}(\mathbf{x}) \le -2\alpha[V(\mathbf{x}) - (E/2\alpha)] \quad (32)$$

where

$$E = -(\hat{\mathbf{v}} - \delta\mathbf{v})^T\{k_c\, n[(1/\epsilon)\hat{\mathbf{v}}] + \mathbf{J}^{-1}\mathbf{h}\} \quad (33)$$

By establishing an upper bound on the parameter E of Eq. (33), condition *(ii)* of Eq. (28) is satisfied by choosing $V^* = \bar{E}/2\alpha$, where $\bar{E}$ is the indicated upper bound, Equation (33) can be further

characterized using the requirements on the function n given in Eq. (25). Using condition (*i*) of Eq. (25), further manipulation of Eq. (33) yields the following expression:

$$E \leq \|\hat{\mathbf{v}}\|[\|\mathbf{h}\|/\varrho(\mathbf{J}) - k_\epsilon\|\mathbf{n}\|] + \|\delta\mathbf{v}\|[\|\mathbf{h}\|/\varrho(\mathbf{J}) + k_\epsilon\|\mathbf{n}\|] \tag{34}$$

By examining the behavior of the quantities appearing in Eq. (34) for a specific vehicle and application, a suitable value of $\bar{E}$ can be established, Condition (*ii*) of Eq. (25) implies that progressively smaller values of c, an argument of the function **n,** result in correspondingly smaller limits on the magnitude of the first bracketed term of E in Eq. *(34).* Given the size of the bounding function k_ϵ established in Eq. (24), the magnitude of this term approaches zero in the limit as c approaches zero. As would bc expected, a decrease in c implies an increase in thruster activity. The practical consequence is a trade between control accuracy and propellant consumption, which is governed by the number and frequency of thruster firings, The second term in Eq. (34) provides an intuitive result, showing that attitude and rate sensing errors, which manifest themselves in $\delta\mathbf{v}$, impose a fundamental limit on the smallest value of E than can actually bc achieved, independent of the value of c selected.

As shown by Corless,[22] a Lyapunov function meeting the stated requirements ensures exponential convergence of the state, x, to within a neighborhood around the origin defined by V(x) $\leq V^*$ (recall that $V^* = \bar{E}/2\alpha$). Using Eqs. (27) and (31), the following expression is obtained for this region:

$$4\alpha^4\Delta\varphi^2 + 2\alpha^2\Delta\dot{\varphi}^2 + 4\alpha^3\Delta\varphi\Delta\dot{\varphi} \leq \bar{E} \tag{35}$$

Once the state has entered the domain specified by Eq. (35), it will remain there indefinitely. Thus, Eq. (35) can be used to portray the limit cycle envelope of the controller graphically, in a manner similar to phase-plane analysis, Although $\Delta\varphi$, as defined in Eq. (11), is positive for computational purposes duc to the convention chosen for the Euler rotation axis in Eq. (12), negative values of $\Delta\varphi$ arc meaningful in this context. A more detailed development of Eqs. (29) through (35) is given by Thurman.[23]

DIGITAL AUTOPILOT DESIGN

The pulse-mode control theory, as presented above, implicitly assumes that the parameters needed to compute torque commands are continuously available, and that those commands are continuously executed without any computational or mechanical delays. However, the theory is applicable to sampled data systems with proper interpretation This section describes the primary considerations in the design of a spacecraft autopilot for digital computer implementation.

Design Parameters

In a sampled data system, the command torque expression of Eq. (9) is evaluated at discrete intervals. Using Eqs. (9), (13), (14), and (17), the following expression is obtained:

$$\mathbf{m}_c(t_k) = \mathbf{K}_P \Delta\hat{\Phi}_k - \mathbf{K}_D \Delta\hat{\omega}_k + \mathbf{K}_\epsilon \mathbf{n}[(1/c)(k_P \Delta\hat{\Phi}_k - k_D \Delta\hat{\omega}_k)] + \mathbf{c}_k \tag{36}$$

In Eq. (36) the subscript k implies the value of the indicated quantity at time t_k. A useful form for the function $\mathbf{n}$ satisfying the conditions of Eq. (25) that mimics the behavior of the thrusters is as follows:

$$\begin{aligned} \mathbf{n}(\epsilon, \hat{\mathbf{v}}) &= \mathbf{0}; \qquad \|\hat{\mathbf{v}}\| < \epsilon \\ \mathbf{n}(\epsilon, \hat{\mathbf{v}}) &= \hat{\mathbf{v}}/\|\hat{\mathbf{v}}\|; \quad \|\hat{\mathbf{v}}\| \geq \epsilon \end{aligned} \tag{37}$$

The key design parameters to be chosen are the rate of convergence, cc, which determines the values of the feedback gains k_P and k_D given in Eq. (31), the parameter c, which sets the thruster firing deadband in Eq. (37), and the interval between command updates, designated T. When designing a model-independent autopilot for a spacecraft that can apply only a single torque level to each axis, a simpler *version* of Eq. (36) can be used, by eliminating the first, second, and fourth terms. These terms must then be treated as part of the vector $\mathbf{h}$ of Eq. (20), along with all other uncompensated or unmodeled dynamical terms. As long the matrix $\mathbf{K}_\epsilon$ in Eq. (36) satisfies Eqs. (23) and (24), the exponential stability criteria of Eq. (28) will hold, with $\mathbf{m}_c(t_k)$ being determined solely by the third term of Eq. (36).

Thruster valve characteristics limit the smallest pulse width for which reliable operation is assured. This effectively sets the smallest usable value of T, and limits control precision to levels commensurate with the angular position and rate changes induced by minimum impulse thruster firings. For sample-and-hold systems, the same logic still applies if a value of T larger than the minimum pulse width is chosen, in that the attitude and rate changes duc to a thruster pulse of T seconds limits the achievable precision, In onc sense a minimum pulse width is beneficial, as it incorporates hysteresis into the digital controller that prevents "chattering" of the thruster salves. For values of T that arc small relative to the frequency range of the spacecraft dynamics, the following expressions arc useful:

$$|A@|_{min} \approx [m/\underline{\sigma}(\mathbf{J})]T$$
$$|\Delta\varphi|_{min} \approx (T/2)|\Delta\dot{\varphi}|_{min} \qquad (38)$$

in Eq. (38), m represents the torque capability of the spacecraft; $\underline{\sigma}(\mathbf{J})$ has the same meaning as in Eq. (24) Equation (38) provides approximate upper bounds on the minimum values of $\Delta\varphi$ and $\Delta\dot{\varphi}$ that can bc achieved for a given T, independent of other error sources, such as high frequency attitude sensor noise., that can also influence the choice of ϵ. The bounds in Eq. (38) provide a guideline for the smallest value of ϵ that will ensure a sufficiently large thruster firing dcadband:

$$\epsilon > k_P|\Delta\varphi|_{min} + k_D|\Delta\dot{\varphi}|_{min} \qquad (39)$$

In addition to sampling rate considerations, time delays between the sampling of attitude sensors and the implementation of thruster firing commands must bc considered. This error source can bc interpreted as a modeling error in Eqs. (18) and (20); its effect will bc addressed further below.

Performance Specifications

In the transient phase of operation, a pulse-nmdc controller based on Eqs. (36) and (37) attempts to force the closed-loop attitude dynamics to approximate the following linear differential equation:

$$\Delta\ddot{\varphi} + k_D\,\Delta\dot{\varphi} + k_P\,\Delta\varphi \approx 0 \qquad \text{(w)}$$

Overall, Eq. (4O) gives the most accurate approximate ion of the transient behavior in rest-to-rest slew maneuvers, in which the angular velocity vector of the spacecraft would ideally bc parallel with the Euler rotation axis over the course of the maneuver. As with Eq. (35), the usc of Eq. (40) as an analytical tool admits negative values of the attitude error angle $\Delta\varphi$. The values of k_P and k_D given in Eq. (31) in terms of the convergence rate α yield the following damping ratio, ζ, and natural frequency, f_n, of the Closed-loop system:

$$\begin{aligned} \zeta &\approx 0.707 \\ f_n &\approx (1/\sqrt{2}\,\pi)\,\alpha \end{aligned} \qquad \textbf{(41)}$$

For the indicated damping ratio, the natural frequency of the system is also equal to its -3 dB bandwidth; hence, the bandwidth is immediately determined by the value of α selected.

Once the spacecraft's attitude state has entered the region specified by Eq. (35), it will exhibit some type of limit cycle behavior thereafter, with the envelope of this region established by the parameter E of Eqs. (33) and (34). For slew maneuvers in which the terminal value of the commanded angular velocity, ω_c, is zero, the following upper bound on E can bc used:

$$E \approx (\epsilon + \xi)(\epsilon + \delta v) \qquad (42)$$

Equation (42) incorporates approximate upper bounds, immediately prior to a thruster firing, on the vector $\hat{\mathbf{v}}$ of Eq. (14), the modeling error vector $\mathbf{h}$ of Eq. (20), and the erroneous angular w.coloration commands of Eq. (22), designated δv. The parameter< bounds thrust implementation errors in Eq. (20) duc to the interval between command computations (T) and any time delays present in the system; in most modern spacecraft control systems, ξ is small compared with the other parameters in Eq. (42?). Using Eq. (42), an accurate estimate of the limit cycle regime can bc obtained from Eq. (35).

MIDCOURSE GUIDANCE COMPUTER SIMU1,ATION

This section describes the simulation of a digital autopilot for midcourse guidance of an interplanetary spacecraft. in this scenario, a hypothetical soft lander approaching the planet Mars performs a late propulsive maneuver to remove residual targeting errors about 30 min prior to atmospheric entry, descent, and landing. The vehicle is similar to the *Mars Pathfinder* spacecraft,[24] which in actual operation executes maneuvers via ground-based commands, rather than onboard control.

Spacecraft Description

The spacecraft configuration during interplanetary flight is shown in Fig. 2. Specific configuration data arc provided in Table 1. The lander is carried to Mars inside an entry vehicle attached to a cruise stage, The cruise stage is equipped with sun sensors and a star tracker for attitude determination, eight thrusters for attitude control and midcourse propulsion, and a solar array for power generation. It should be noted that the plane containing the roll thrusters is offset from the spacecraft's center of mass about 10 cm The thruster configuration, while efficient, provides the capability for coupled torques only about the roll axis; pitch and yaw thruster firings yield both torques and translational velocity changes. The lander carries a strapdown Inertial Measurement Unit (IMU) which is used to perform inertial navigation during midcourse maneuvers and the terminal descent phase.

A high-level block diagram of the spacecraft's midcourse guidance system is shown in Fig. 3. The key parameters of the digital autopilot arc given in Table 2. A velocity-to-bc-gained method is used for guidance,[25] in which the spacecraft maneuvers itself to null the velocity-to-bc-gained vector, representing the difference between the velocity required to achieve the proper atmospheric entry conditions and the velocity indicated by the inertial navigation system. At each command interval (the subscript k in Fig. 3 signifies the value of the indicated parameter at time t_k), the guidance law supplies the autopilot with the velocity-to-bc-gained and a commanded attitude quaternion that will align the thrust axis (the x axis in Fig. 3) with the velocity-to-bc-gained vector, These quantities, along with

estimates of the current attitude quaternion and angular velocity vector obtained from the navigation system, arc used to determine the command torque vector.

The autopilot employs a simple model-indcpcndcnt pulse-mocic controller. The commanded torque is computed using the third term of Eq. (36) and Eq. (37), as described previously; this computation is also illustrated in Fig. 3. The matrix $\mathbf{K}_\epsilon$ of Eq. (36) is diagonal, with the values on the diagonal being the nominal torque generated about the x, *y*, and z spacecraft body axes, respectively, by the appropriate thruster firings These values are labeled m_x, m_y, and m_z in Table 2. At each command interval, the autopilot issues commands to the thruster valves only when a change in the state of a given thruster is needed. When the guidance system senses that the spacecraft is within the limit cycle envelope of Eq. (35), the thrusters arc used to carry out velocity changes. During these periods, certain thrusters may bc turned off momentarily, when torque commands for attitude maintenance arc issued.

The thruster characteristics given in ~'able 1 arc represent ative of modern bipropellant engines for small spat..ccrail propulsion.[26] Engines of this type, using nitrogen tetroxide and monomethyl hydrazine, deliver a specific impulse of 300 to 320 s. The error mode] used to represent the inertial navigation system is summarized in Table 3. The I MU contains three ring-laser gyroscopes and three pendulous accelerometers; its performance is represent ative of the strapdown 1 MUS carried by the *Clementine* spacecraft.[27] The error model components in Table 3 arc based on established modeling techniques for these instruments.[28] The navigation system is initialized with ground-based estimates of the spacecraft's position and velocity vectors relative to Mars;[29] the initial attitude quaternion is established by an alignment process performed onboard the spacecraft using its att itudc sensors. The bias errors of the gyroscopes and accelerometers arc also calibrated during the alignment process.

Mission Scenario

The sequence of events for the maneuver is illustrated in Fig. 4. Alignment and initialization of the inertial navigation system is done with the spacecraft three-axis stabilized in its nominal entry attitudc.

After receipt of an enable command from the ground, the autopilot slews the spacecraft to align its thrust (+x) axis with the indicated vc]ocity-to-bc-gained vector. Since the spacecraft's pitch and yaw thrusters arc unbalanced, the commanded attitude changes slightly (a fcw degrees) during this slew maneuver, due to the change in the velocity-to-bc-gained resulting from velocity changes induced by unbalanced thruster firings, Once the guidance system senses that the spacecraft has entered the limit cycle envelope about the commanded attitude, the autopilot uses the pitch and yaw thrusters to perform the commanded velocity change and to hold the spacecraft in the correct burn attitude simultaneously. Before the initiation of this burn, the velocity-to-be-gained vector computed by the guidance law is intentionally biased so that after the spacecraft returns to its initial attitude a small residual value remains, with a direction that will always have components which can be nulled by a combination of pitch/yaw and roll thruster firings,

After the primary burn is completed, the autopilot reorients the spacecraft back to its initial attitude. During this reorientation maneuver, the spacecraft's roll angle is adjusted so that the residual velocity-to-bc-gained vector lies in the plane containing the thrust axes of the roll and yaw thrusters. Finally, the autopilot performs a small trim bum while maintaining the spacecraft in its initial attitude, which nulls the residual velocity-to-be-gained induced by the velocity change of the reorientation maneuver and the bias applied to the primary burn. When firing the roll thrusters to execute velocity changes, the autopilot uses the pitch thrusters to maintain the spacecraft's attitude against the resulting disturbance torques. With this procedure, the autopilot can perform a midcourse maneuver very accurately, without the need for open-loop compensation of the velocity changes caused by using unbalanced thruster firings for attitude control.

Digital Simulation

The dynamics of the spacecraft were simulated by numerical integration of the six-degree-of-freedom equations of motion, treating the vehicle as a rigid body with variable mass and moments of

inertia. No external disturbances, such as solar radiation pressure-induecd torques, were modeled, duc to their negligible size compared with the disturbances induced by propulsion system operation and center of mass offsets. Integration was accomplished using a 70' order Runge-Kutta formula with 8th order step size control, with all computations done in double precision arithmetic. The nominal integration t imc step was 20 ms, while the tolerance used to trigger time step adjustments was set to onc part in 1010. The initial mass and inertia tensor were generated using a pseudo-random number generator, according to Gaussian distributions with the statistics specified in Table 1. Center of mass modeling and calibration errors were also simulated in a similar manner, with the center of mass offset statistics of Table 1 applying to both they and z axes of the spacecraft.

Thrust level variations between successive thruster firings were simulated by pseudo-random Gaussian number generation for each individual thruster, again using the statistics given in Table 1, Navigation errors were simulated by numerical integration of the appropriate error equations (the interested reader is referred to the text by Britting[30] for a derivation of strapdown inertial navigation error equations), using pseudo-random number generation to sample the statistics of the error sources described in Table 3. Due to the relatively slow variation of the navigational errors, these parameters were integrated in double precision arithmetic using a 4th order, fixed step Runge-Kutta formula with a step size of 20 ms, The time delays associated with thruster valve operation and computer operation were also simulated, using the values given in Tables 1 and 2. The computational time delay, designated δT in Table 2, was based on an approximate count of the number of operations during each command cycle. An average value of the time needed to perform these operations on several modern space-qualified microprocessors was then determined

Results

The attitude and velocity-to-bc-gained history of a simulated maneuver arc shown in Figs. 5 and 6, respectively. 't'his case represents a relatively difficult scenario: the spacecraft must rapidly slew

almost 180 deg, execute a velocity change of 7.2 m/s to correct a 13 km targeting error, then return to its initial attitude. For illustrative purposes, the attitude of the spat.cmaft is characterized in Fig. 5 by three Euler angles; these are heading (ψ), pitch (θ) and roll (ϕ). The order of rotation for the body axes of Fig. 2 from the Mars-centered coordinate frame used by the navigation system to the current attitude is a rotation of angle ψ about the yaw ($+z$) axis, followed by a rotation of angle θ about the pitch ($+y$) axis, then a rotation of angle ϕ about the roll ($+x$) axis, The values of these angles corresponding to the commanded attitude, designated ψ_c, θ_c, and ϕ_c, respectively, arc also shown in Fig. 5.

'l-hc actual components of the velocity-to-bc-gained vector and those computed by the navigation system arc shown in Fig, 6. The components of these vectors arc specified in a Mars-centered, nonrotating, mean equator of epoch 2000.0 coordinate system. In this system, the x and y axes arc parallel to the Martian equatorial plane, while the z axis is normal to this plane and parallel to the mean spin axis of Mars at the indicated epoch, The flight path followed by the spacecraft during the period of interest is such that its velocity vector is nearly aligned with they-z plane, pointing in roughly the -y direction, but inclined at an angle of about 20 deg below the equatorial (x-y) plane, Differences between the actual and indicated vckwity-to-bc-gained components seen in Fig. 6 arc duc to errors in both the position and velocity vectors computed by the navigation system.

The roll, pitch, and yaw thruster firings during the first ten seconds of the maneuver arc shown in Fig. 7. Note that though the autopilot computes commands at a SO-HZ rate, the highest pulse frequency seen in Fig. 7 is only about 7 Hz for the yaw thrusters, and 1 to 4 Hz for the pitch and roll thrusters, In comparison, the lowest vibrational frequency of the spacecraft structure is approximately 20 Hz. As suggested by Eqs. (40) and (41), the autopilot is attempting to approximate a specified linear system by varying the frequency and width of the thruster pulses to approximate, in an average sense, a proportional-phrs-derivative commanded torque profile. This behavior is similar to that of the integral pulse-frcqucney controller of Farrenkopf *et al.*[2] The additional advantage possessed by the autopilot of

Fig. 4 is that with pulse-width and pulse-frequency modulation, the number of thruster valve cycles during the slew maneuvers is reduced.

According to Fig. 5, the initial turn takes about 67 s to complete, In comparison, an analytical prediction of the time required to reach the commanded attitude, based on Eqs. (26), (35), and (42), was 68 s. The primary bum takes about 190s to complete, employing all four pitch and yaw thrusters. The attitude history of the reorientation maneuver following the primary burn shows that the commanded roll angle ϕ_c changes rapidly during the first 20 seconds, The autopilot follows this change, although reorientation takes about 80s as opposed to 67s for the initial turn. Even though the commanded torque formula contains no feedforward term ($\dot{\omega}_c$), the autopilot is still able to track the commanded attitude, without the need for gain scheduling, The two slew maneuvers and the trim burn generate velocity changes with a combined magnitude of about 0.5 m/s, This represents an overhead of *7%* in propellant consumption compared with the net 7.2 m/s velocity change of the maneuver. If needed, this overhead could be reduced by doing the slew maneuvers more slowly.

The thruster firing deadband used to establish the cutoff point for velocity changes, designated y in Table 2, is *2%* of the commanded velocity change. This cutoff condition is applied to both the primary bum and the trim burn, Residual velocity-to-be-gained components remaining after the trim burn arc less than 4 rinds; this corresponds to a precision of about 0.05% in executing the maneuver. The overall maneuver execution error is about 10%, due entirely to the effect of navigational errors.

ACKNOWLEDGMENTS

The research described in this paper was carried out, in part, at the Jet Propulsion Laboratory, California Institute of Technology, under contract with the National Aeronautics and Space Administration, The authors extend their thanks to Mr. David Spencer of Jet Propulsion Laboratory, for providing *Mars Pathfinder* trajectory and targeting data used in the digital computer simulations.

REFERENCES

1. Gaylord, R. S., and W. N. Keller, "Attitude Control System Using Logically Controlled Pulses," *Progress in Astronautics and Rocketry*, Vol. 8, R. E. Roberson and J. S. Farrior, Eds., Academic Press, New York, 1962, pp. 629-648.

2. Farrenkopf, R, L., Sabroff, A. E., and P. C. Wheeler, "Integral Pulse Frequency On-Off Control," *Progress in Astronautics and Aeronautics,* Vol. 13, R. C. Langford and C. J. Mundo, Eds., Academic Press, New York, 1964, pp. 185-230.

3. Dahl, P. R., Aldrich, G. T., and L. K. Herman, "Limit Cycles in Reaction Jet Attitude Control Systems Subject to External Torques," Progress *in Astronautics and Rocketry*, Vol. 8, R. E. Roberson and J. S. Farrior, Eds., Academic Press, New York, 1962, pp. 599-627.

4. Haloulakos, V. E., "Analysis of Jet Attitude Control Systems Subject to Varying Magnitudes of External Disturbing Torques," AIAA Paper 67-537, AIAA Guidance, Control, and Flight Dynamics Conference, Huntsville, Alabama, Aug. 1967.

5 Martin, F. H., and R. H. Battin, "Conlputm-Controlled Steering of the Apollo Spacecraft," *Journal of Spacecraft and Rockets,* Vol. 5, No, 4, Apr. 1968, pp. 400-407.

6. Widnall, W. S., "Lunar Module Digital Autopilot,'' Journal *of Spacecraft and Rockets*, Vol. 8, No. 1, Jan. 1971, pp. 56-62.

7. Ingoldby, R, N., "Guidance and Control System Design of the Viking Planetary Lander," *Journal of Guidance and Control,* Vol. 1, No. 3, May-Jun. 1978, pp. 189-196,

8. Bergmann, E. V., Croopnick, S. R., Turkovich, J. J., and (. C. Works, "An Advanced Spacecraft Autopilot Concept," *Journal of Guidance and Control*, Vol. *2,* No. 3, May-Jun. 1979, pp. 161-168.

9. D'Amario, L. A,, and G, S. Stubbs, "A Ncw Single-Axis Autopilot for Rapid Spacecraft Attitude Maneuvers," *Journal of Guidance and Control,* Vol. 2, No. 4, Jul.-Aug. 1979, pp. 339-346.

10. Dwyer, T. A. W,, 111, "Exact Nonlinear Control of Large Angle Rotational Maneuvers," *IEEE Transactions on Automatic Control*, Vol. AC-29, No, 9, Sep. 1984, pp. 769-774.

11. Wit, B., and P. M. Barba, "Quaternion Feedback for Spacecraft Large Angle Maneuvers," *Journal of Guidance, Control, and Dynamics*, Vol, 8, No, 3, May-Jun. 1985, pp. 360-365.

12 Wie, B., Weiss, H., and A. Arapostathis, "A Quaternion Feedback Regulator for Spacecraft Eigenaxis Rotations," *Journal of Guidance, Control, and Dynamics*, Vol. 12, No. 3, May-Jun. 1989, pp. 375-380.

13. Wen, J. T.-Y., and K. Kreutz-Delgado, "The Attitude Control Problem," *IEEE Transactions on Automatic Control*, Vol. AC-36, No. 10, Oct. 1991, pp. 1148-1162.

14. Weiss, H., "Quaternion-Based Rate/Attitude Tracking System with Application to Gimbal Attitude Control," *Journal of Guidance, Control, and Dynamics*, Vol. 16, No. 4, Jul.-Aug. 1993, pp. 609-616,

15. Corless, M., "Control of Uncertain Nonlinear Systems," *Journal of Dynamic Systems, Measurement, and Control,* Vol. 115, Jun. 1993, pp. **362-372.**

16. Leitmann, G., "On One Approach to the Control of Uncertain Systems," *Journal of Dynamic Systems, Measurement, and Control,* Vol. 115, Jun. 1993, pp. 373-380.

17. Thurman, S. W., and H. Flashner, "A New Pulse-Modulation Technique for Guidance and Control of Automated Spacecraft," manuscript submitted to *Journal of Guidance, Control, and Dynamics.*

18. Utkin, V. 1, , *Sliding Modes and Their Application to Variable Structure Systems,* MIR, Moscow, 1978.

19. Slotine, J. J., and W. Li, *AppliedNonlinear Control,* Prentice-Hall, Englewood Cliffs, New Jersey, 1991, pp. 276-307.

20, Hughes, P. C., *Spacecraft Attitude Dynamics*, Wiley, New York, 1986.

21. Wertz, J. R., Ed., *Spacecraft Attitude Determination and Control*, D. Reidel, Dordrecht, The Netherlands, 1978.

22 Corless, M,, "Guaranteed Rates of Exponential Convergence for Uncertain Systems," *Journal of Optimization Theory and Applications,* Vol. 64, No. 3, Mar, 1990, pp. 481-494.

23. Thurman, S. W., "A Comprehensive Pulse-Modulation Theory for Guidance and Control of Automated Spacecraft," Ph.D. Dissertation (in preparation), University of Southern California, Los Angeles, California, May 1995.

24. *Mars Pathfinder Mission Plan*, JPL Document D-11355 (internal document), Jet Propulsion Laboratory, Pasadena, California, December 1993.

25. Battin, R. H., *An Introduction to the Mathematics and Methods of Astrodynamics*, AIAA Education Series, New York, 1987, pp. *550-566.*

26 Rosenberg, S. D., and L. Schoenman, "New Generation of High-Performance Engines for Spacecraft Propulsion," *Journal of Propulsion and Power*, Vol. 10, No, 1, Jan. -Feb. 1994, pp. *40-46,*

27. DeLaHunt, P., Gates, S., Levenson, M,, and G. Creamer, "The Clementine Attitude Determination and Control System," Proceedings of the 8th Annual AIAA/Utah State University Conference on Small Satellites, Logan, Utah, Aug. 1994,

28. Savage, P. G., "Strapdown Sensors," *Strapdown Inertial Systems,* North Atlantic Treaty organization AGARD Lecture Series No, 95, National Technical Information Service, Springfield, Virginia, Jun. 1978,

29. Thurman, S. W., and V. M. Pollmeier, "Guidance and Navigation for the Mars Pathfinder Mission," *Acts Astronautic,* Supplement to Vol. 35, 1995, pp. S45-5S4.

30. Witting, K. R., *Inertial Navigation Systems Analysis,* Wiley, New York, 1971, pp. 153-194.

Table 1: Spacecraft Configuration Data ‘

Parameter	*Nominal Value*	*RMS (1σ) Variation*
Initial Mass		
spacecraft (dry), **kg**	*420.0*	**0.5%**
propellant/oxidizer, kg	**30.0**	**2.0%**
Initial Moments of Inertia		
yaw (z-axis), kg-m^2	**120.0**	2.0?40
pitch (y-axis), kg-m^2	**115.0**	**2.0%**
roll (x-axis), kg-m^2	**145.0**	2.0%
cross-products, kg-m^2	< 5.0	—
Center of Mass Offset, cm	**0.0**	**1.0**
Thruster Specifications		
thrust level, N	**4.45**	**3.0%**
min pulse width, ms	**20**	—
rise time, ms	**2.0**	—
decay time, ms	**3.0**	—
valve open) close delay, ms	**3.0**	—
max acceleration, m/s^2	**0.04**	2.5%
max pitch/yaw acceleration, rad/s^2	**0.038**	**3.6%**
max roll acceleration, rad/s^2	**0.067**	**2.9%**

Table 2: Digital Autopilot Parameters

Parameter	Description	Value
T	command update interval	20 ms
δT	computation time required for each command update	3 ms
γ	guidance thruster firing deadband	2% of ΔV
Attitude Control		
a	attitude error rate of convergence	0.0765 s^{-1}
m_x	roll axis torque level	9.8 N-m
m_y	pitch axis torque level	4.45 N-m
m_z	yaw axis torque level	4.45 N-m
k_D	angular rate feedback gain	0.153 s^{-1}
k_P	angular position feedback gain	0.0117 S^{-2}
k_v	Lyapunov function parameter	1.8×10^{-3} s^{-3}
ϵ	attitude thruster firing deadband	2×10^{-4} s^{-2}

Table 3: Inertial Navigation System Error Model

Parameter	*RMS (1σ) Value*	*Units,*
Initial Position Error	**0.18** (x) **4.00 (y)** **5.26** (z)	**km**
Initial Velocity Error	*0.06* (x) **0.24 (y)** **0.01 (z)**	m/s
Initial Attitude Error	**0.1 (each axis)**	**deg**
IMU Misalignment	**18**	arcsec
Gyro Error Mod el		
turn-on bias repeatability	**1.0**	deg/hr
bias calibration error	**0.10**	deg/hr
time-varying bias"	**0.05**	deg/hr
scale factor error	**100**	**ppm**
time-varying scale factor'	**25**	**ppm**
scale factor asymmetry.	**10**	**ppm**
time-varying asymmetry	**10**	**ppm**
random walk	**0.10**	deg/hr$^{1/2}$
Accelerometer Error Model		
turn-on bias repeatability	**500**	µg
bias calibration error	**50**	µg
scale factor error	100	ppm
scale factor asymmetry	**25**	**ppm**
compliance (9^2)	**1.0**	µg/g^2
white noise	1.0	mm/s

"modeled as first-order Gauss-Markov processes wtth time constants of 1 hr

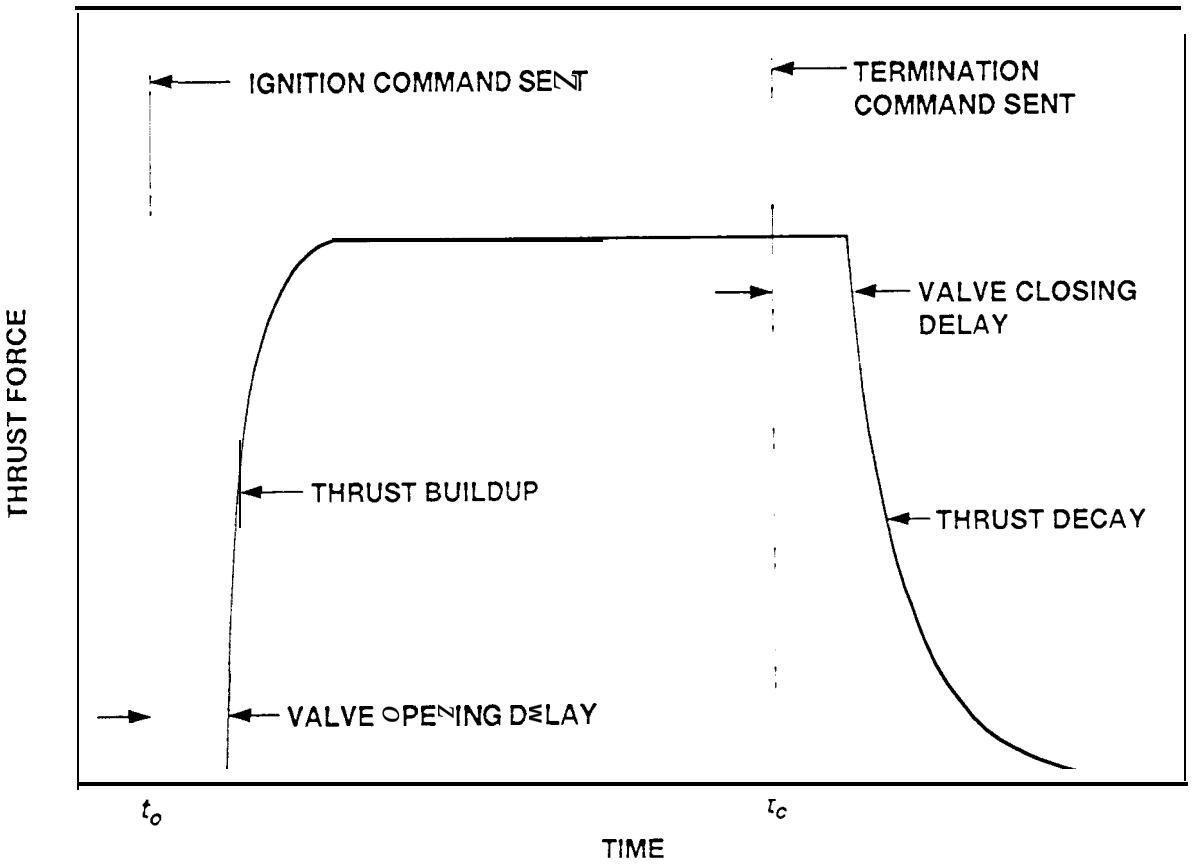

Figure 1: Thruster Firing Profile

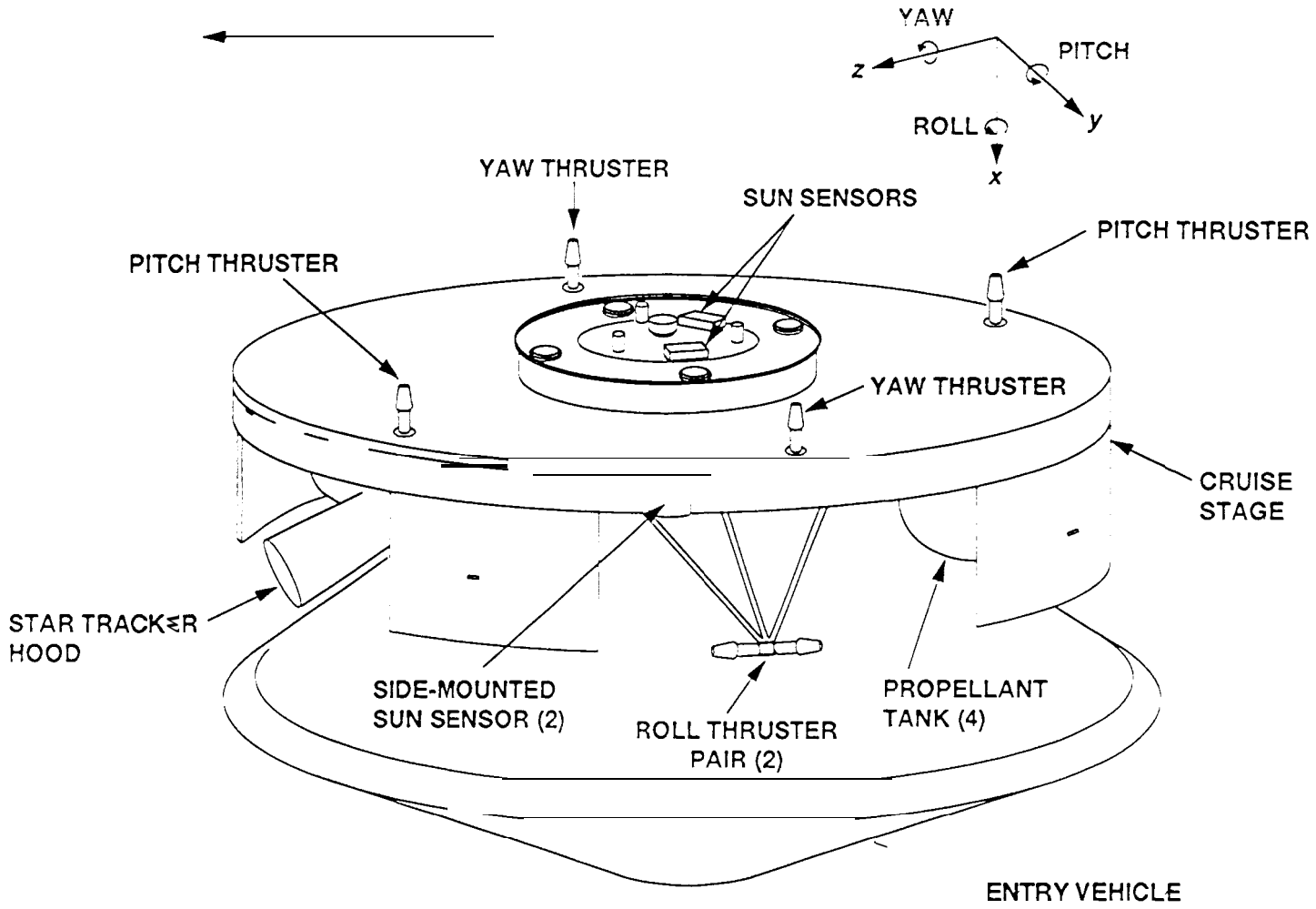

Figure 2: Spacecraft Configuration

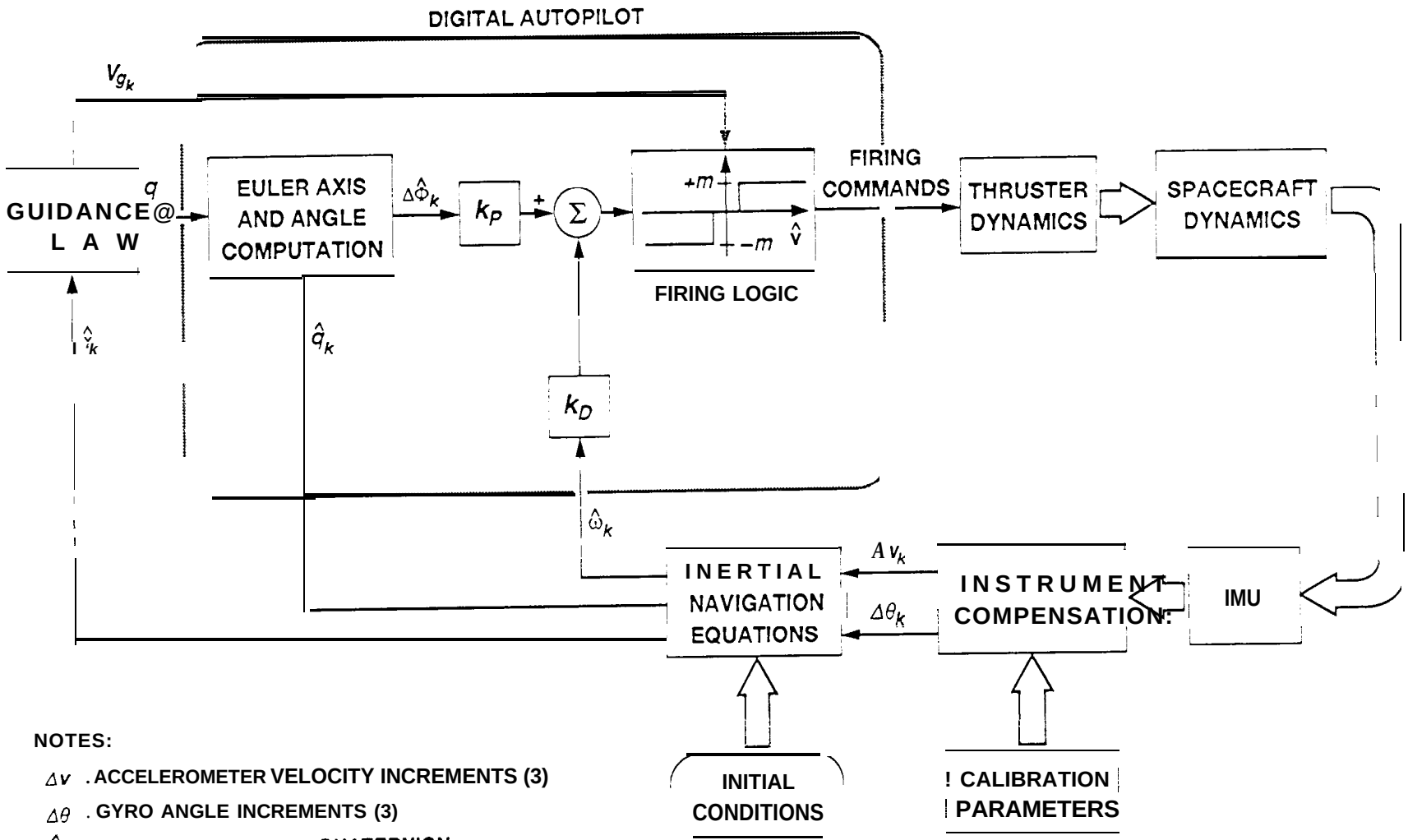

NOTES:

- Δv . ACCELEROMETER VELOCITY INCREMENTS (3)
- $\Delta\theta$. GYRO ANGLE INCREMENTS (3)
- $\hat{q}$ = INDICATED ATTITUDE QUATERNION
- $\hat{\omega}$. INDICATED ANGULAR VELOCITY VECTOR
- $\hat{x}$. INDICATED STATE VECTOR (POSITION/VELOCITY)
- V_g . VELOCITY-TO-BE-GAINED VECTOR
- q_c . COMMANDED ATTITUDE QUATERNION
- $\Delta\hat{\Phi}$. ATTITUDE ERROR VECTOR

Figure 3: Midcourse Guidance System

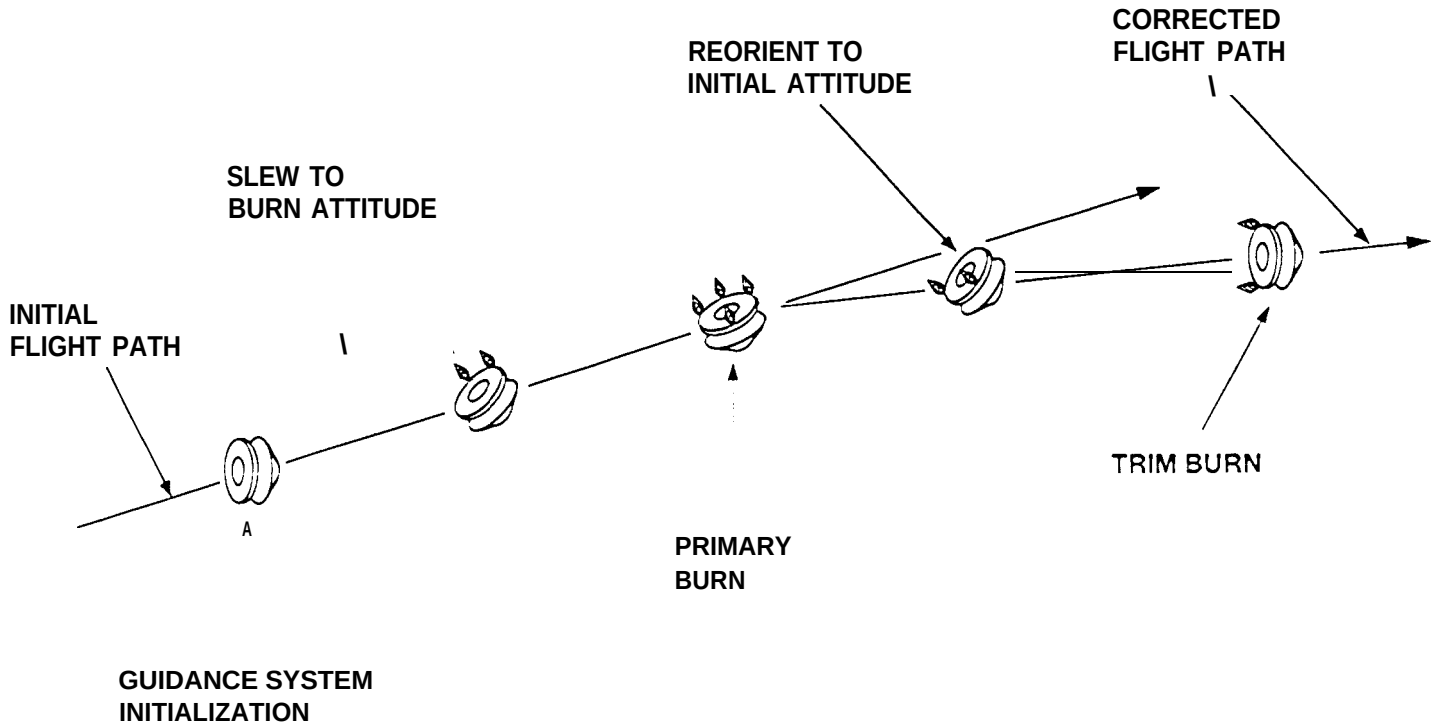

Figure 4: Midcourse Maneuver Profile

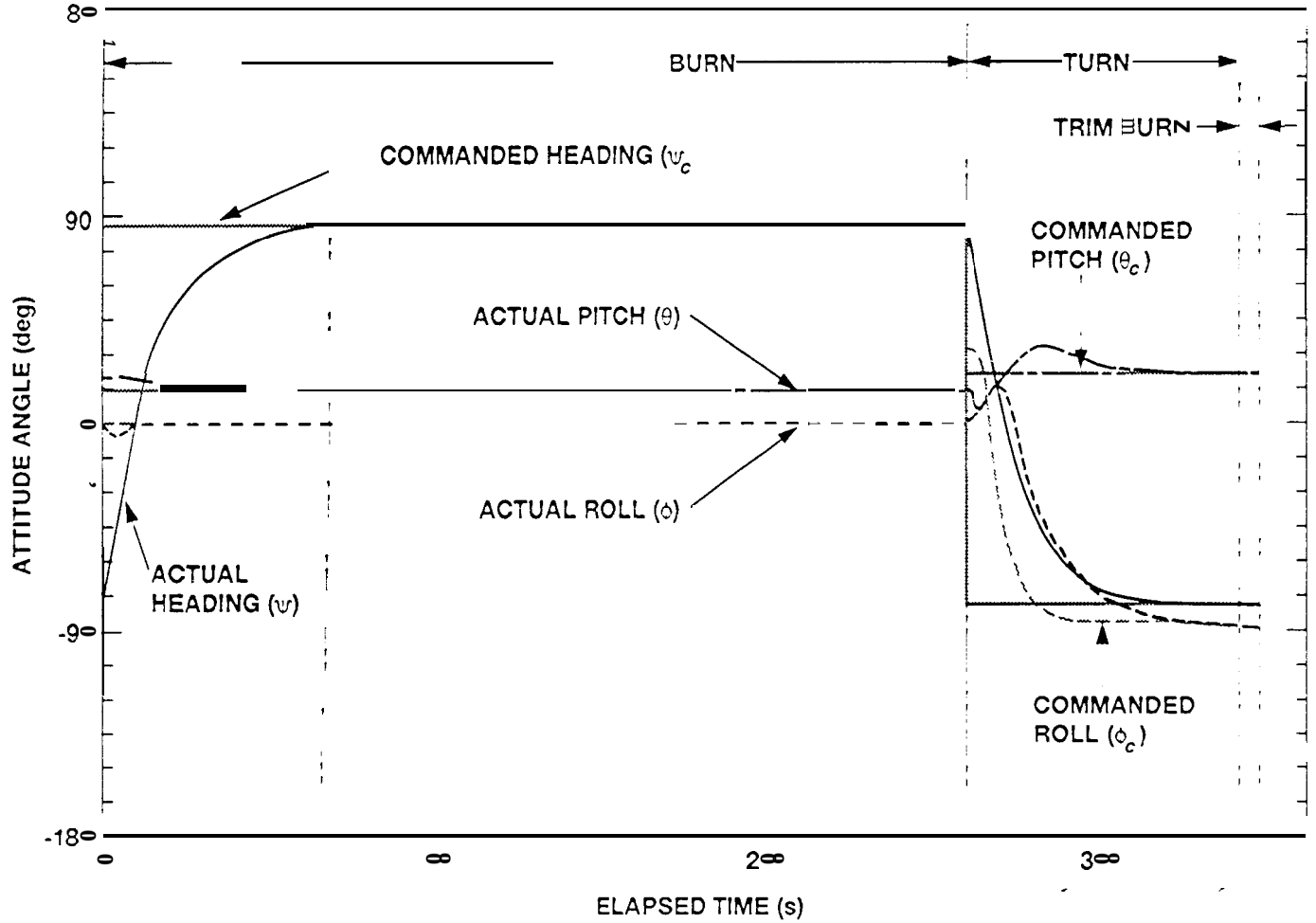

Figure 5: Attitude Angle History

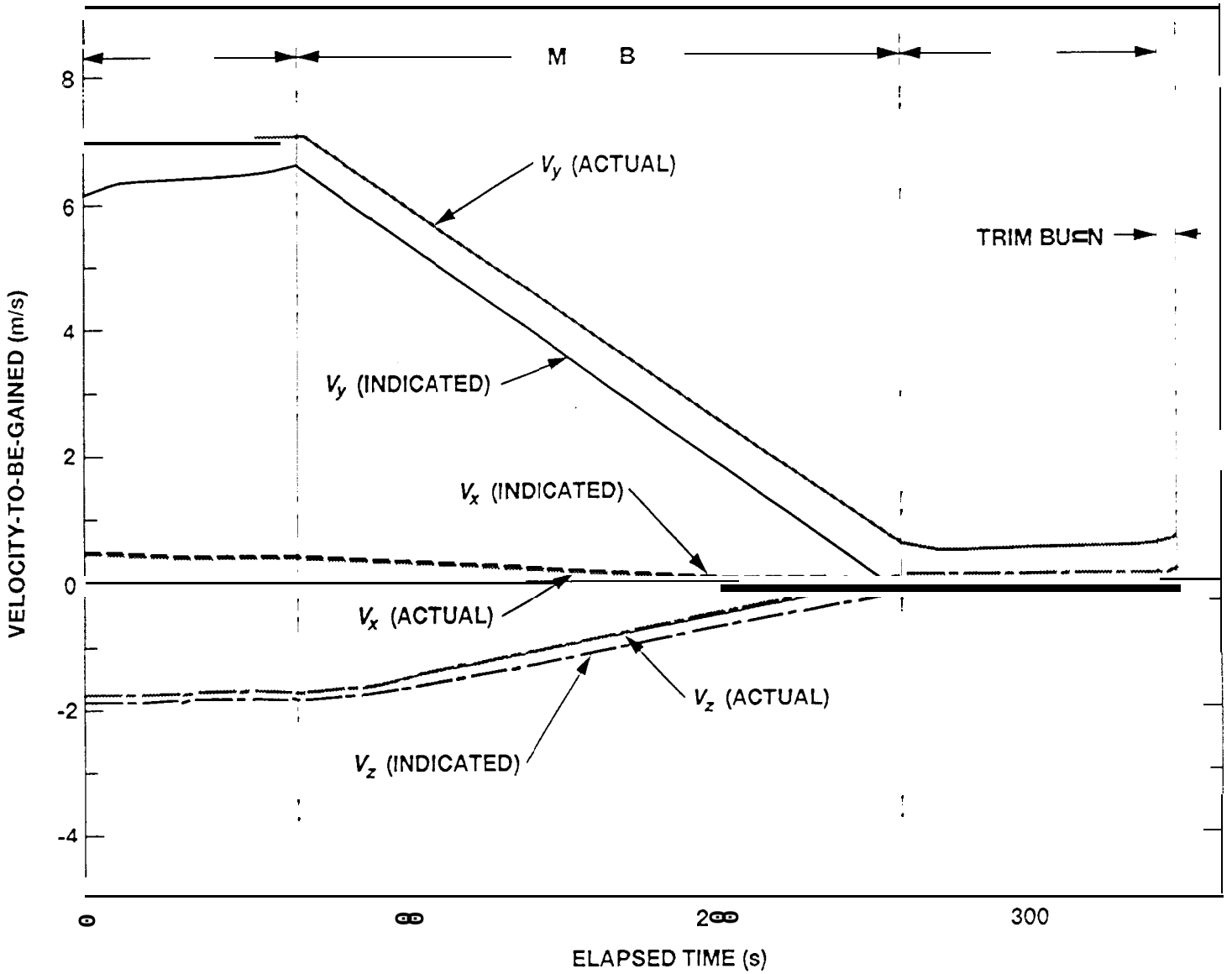

Figure 6: Velocity-to-be-Gained History

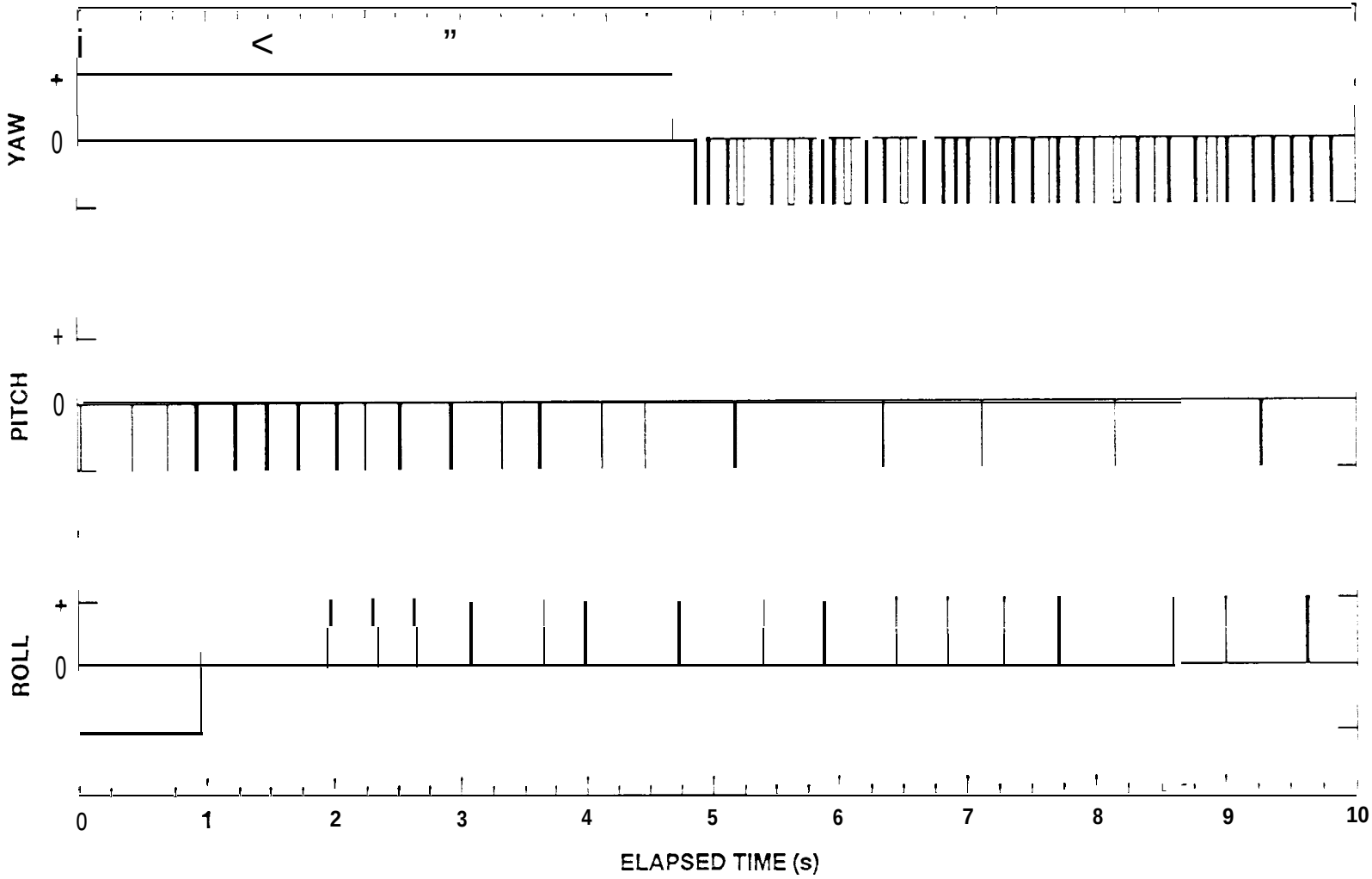

Figure 7: Thruster Firing Partial History